

Broadband Noise Predictions on the ACAT1 Fan Stage Using Large Eddy Simulations and Analytical Models

Danny Lewis*, Stéphane Moreau† and Marc C. Jacob‡

Univ Lyon, Ecole Centrale de Lyon, INSA Lyon, Université Claude Bernard Lyon I, CNRS, Laboratoire de Mécanique des Fluides et d'Acoustique, UMR 5509, 36 Avenue Guy de Collongue, F-69134, Ecully, France

The present paper assesses turbulent flow through and the noise radiation by the "ACAT1" fan stage, which was experimentally tested at the Universal Fan Facility for Acoustics (UFFA) of AneCom AeroTest (ACAT) as part of the European project TurbonoiseBB. The present study focuses on a short-gap configuration, at approach condition, on a so-called Sea Level Static (SLS) working line. Its main objective is to analyze and predict the broadband noise resulting from the impact of the fan wakes onto the Outlet Guide Vane (OGV), also called Rotor-Stator Interaction (RSI) noise. This is achieved *via* a Large Eddy Simulation (LES) of the full fan-OGV stage that is overall in very good agreement with the test performance parameters and with the interstage hot-wire measurements. An in-depth analysis of the multiple flow features is carried out and leads to the identification of the mechanisms at stake in the broadband noise production. The noise is then estimated using two different hybrid approaches. On the one hand, the analytical approach uses an analytical model informed with flow parameters retrieved from the LES. On the other hand, a numerical approach couples the source predicted by the LES with the free-field sound propagation by the Ffowcs Williams and Hawkings (FW-H) analogy. Regarding the analytical approach, Hanson's and Posson's cascade models have been used to perform the broadband RSI noise predictions. The shape of the estimated noise spectra obtained from these models is relatively similar to those of the experimental acoustic power spectra. However, depending on the analytical model and the turbulence lengthscale estimate, some discrepancies on the absolute noise levels may appear. The FW-H analogy recovers the overall shape of the experimental spectra with an overestimation of the radiated noise that is mainly attributed to the fact that the duct propagating properties are neglected by the free-field FW-H analogy. Both the analytical and the numerical noise prediction methodologies eventually suggest that additional non-negligible noise sources might be present in both the experiment and the simulation.

I. Nomenclature

Acronyms

<i>2D</i>	=	Two dimensional.
<i>3D</i>	=	Three dimensional.
<i>ACAT1</i>	=	Fan rig.
<i>CFD</i>	=	Computational Fluid Dynamics.
<i>FW – H</i>	=	Ffowcs Williams and Hawkings.
<i>HW</i>	=	Hot Wire.
<i>IGV</i>	=	Inlet Guide Vane.
<i>LE</i>	=	Leading Edge.
<i>LES</i>	=	Large Eddy Simulation.
<i>LN</i>	=	Low Noise.

*PhD candidate, Ecole Centrale de Lyon, LMFA, danny.lewis@ec-lyon.fr.

†Professor, Ecole Centrale de Lyon, LMFA, AIAA Lifetime Member.

‡Professor, Ecole Centrale de Lyon, LMFA, AIAA Member.

<i>NSCBC</i>	=	Navier-Stokes Characteristic Boundary Conditions.
<i>OGV</i>	=	Outlet Guide Vane.
<i>PSD</i>	=	Power Spectral Density.
<i>SWL</i>	=	Sound Power Level.
<i>RANS</i>	=	Reynolds Averaged Naviers-Stokes.
<i>RSI</i>	=	Rotor Stator Interaction.
<i>SDT</i>	=	NASA Source Diagnostic Test.
<i>SLS</i>	=	Sea Level Static.
<i>TE</i>	=	Trailing Edge.
<i>TI</i>	=	Turbulence Intensity.
<i>TKE</i>	=	Turbulence Kinetic Energy.
<i>TLS</i>	=	Turbulence Length Scale.
<i>UHBR</i>	=	Ultra High Bypass Ratio.
<i>URANS</i>	=	Unsteady Reynolds Averaged Navier-Stokes.
<i>WALE</i>	=	Wall-Adapting Local Eddy-viscosity.
<i>WND</i>	=	Wave Number Decomposition.

subscripts

<i>rms</i>	=	Root mean square.
<i>p</i>	=	Pope estimate (int. length scale).
<i>j</i>	=	Jurdic estimate (int. length scale).
<i>c</i>	=	Auto-correlation based estimate (int. length scale).

II. Introduction

The fan-Outlet Guide Vane (OGV) stage of aircraft engines is currently being considered as one of the major contributors to the total noise radiated by an aircraft, particularly at approach and take-off operating conditions. This trend will intensify with the future Ultra High Bypass Ratio (UHBR) engine architecture, which will be characterized by an increased bypass ratio resulting from a larger diameter. To meet the increasingly stringent noise regulation requirements, significant progress has already been achieved by aircraft manufacturers. Most of them are related to the tonal component of the fan-OGV stage noise, which has been reduced thanks to an intensive use of acoustic liners and a smart blade/vane count selection exploiting the duct cut-off properties. However, little progress has been made in reducing the broadband component of the noise. It originates from stochastic phenomena involving the interaction of turbulent structures with solid surfaces such as walls, blades and vanes. The main mechanism responsible for both broadband and tonal noise generation is the rotor-stator interaction (RSI) which consists in the impingement of the rotor turbulent wakes onto the stator, generating an unsteady loading on the vanes. Additionally, in a near future this mechanism will be all the more dominant since the fan-OGV spacing in UHBR engines will be reduced for the sake of engine performance. This mechanism has been extensively studied over the past few years, using multiple approaches which are gathered in Moreau [1], Moreau *et al.* [2] and Peake *et al.* [3].

To bypass the prohibitive CPU cost of Direct Numerical Simulations, hybrid methods have been developed to carry out studies on the RSI mechanism at a more reasonable cost. These methods are generally a two-step process which separates the computation of the acoustic sources from the propagation. The present paper focuses on the two following hybrid approaches:

- 1) Analytical/Semi-analytical approach: this method couples a CFD computation with an analytical model. The flow parameters that characterize the impinging flow are extracted from the CFD simulation to feed the analytical model which computes the resulting unsteady loading. The latter is then considered as an equivalent dipole source in an acoustic analogy in order to compute the associated radiated noise [4–6]. This approach only requires flow simulations using statistical turbulence models (RANS, URANS), making it possible to compute the RSI noise at an affordable cost especially in an industrial context. Nevertheless, the inherent assumptions made in the turbulence models and the necessary geometry simplifications of the models induce a loss of accuracy.

These models may also be applied to mean flow data extracted from high-fidelity unsteady simulations (such as Large Eddy Simulation - LES), for comparison purposes, although such unsteady simulations are not meant to feed statistical models in the first place.

- 2) Numerical approach [4] : this method couples a fully unsteady flow computation, an LES in the present study, with an acoustic analogy such as the Ffowcs Williams and Hawkings [7] free field analogy, or the Goldstein [8] duct analogy to recover the acoustic far field. These flow simulations enable to directly compute the unsteady loading on the vane, the accuracy of which being set by the mesh itself. The main drawback of such hybrid approaches is that the Green’s function is only known for canonical cases (free-field, uniform flow, annular cylindrical ducts, with possible but complex extensions to slowly varying ducts, lined ducts, mean swirl flows). As a consequence, some specific features such as shear flows are ineluctably neglected in the wave propagation, with a possible impact on the accuracy of the method.

The objective of the present paper is to assess the capacity of the two aforementioned methods to carry out reliable predictions of the broadband RSI noise. It proposes an extensive use of the coupling of LES with both analytical models and acoustic analogies. This study is an alternative to the work previously performed by Lewis *et al.* [9], which focused on RANS-informed analytical models only. The LES as well as the broadband noise predictions have all been performed on the ACAT1 configuration tested in 2018 in the ANECOM UFFA facility in Wildau (Germany) in the framework of the European project TurbonoiseBB [10–13]. An in-depth analysis of the flow physics is conducted in order to understand more precisely the RSI mechanism and to assess the validity of some assumptions made within the analytical models.

III. Benchmark configuration

The ACAT1 turbofan model consists of 20 fan blades and 44 stator vanes. Two configurations have been tested: one with a short inter-stage and an additional one with a longer inter-stage (Fig. 1). Both configurations were tested at different operating conditions (approach, side-line and cut-back conditions) on two different working lines (SLS and LN) that differ by the blade loading of the fan. The present paper focuses exclusively on the SLS working line, at approach condition, for the short inter-stage configuration. The flow conditions of this operating point are given in Table 1.

Rotation speed (rpm)	3828.2
Tip relative Mach number	0.57
Total mass-flow rate (<i>kg/s</i>)	55.156
Bypass ratio	7.6
Ambient pressure (hPa)	995.6
Ambient temperature (K)	292.8

Table 1 Approach condition.

IV. Simulations set-up

A. Computational domain

1. LES computational domain

In order to limit the computational costs of the simulation, computational domains for turbomachines are commonly reduced using periodic boundary conditions. In the particular case of the TurboAVBP solver used in the present study, the rotor-stator interface requires to have the same angular sector for the rotor and stator domains. For the ACAT1 geometry, the domain can thus be reduced to a quarter of the geometry, consisting of 5 fan blades and 11 vanes. Nevertheless, a 5-11 domain is still too large for a complete hub-to-tip fan/OGV LES. To further reduce the computational domain, a modification of the vane count, reducing it from 44 to 40 (10% reduction), has been performed. This has resulted in a 1 rotor blade-2 stator vane configuration ($2\pi/20$ periodicity), which allows to significantly reduce the computational costs.

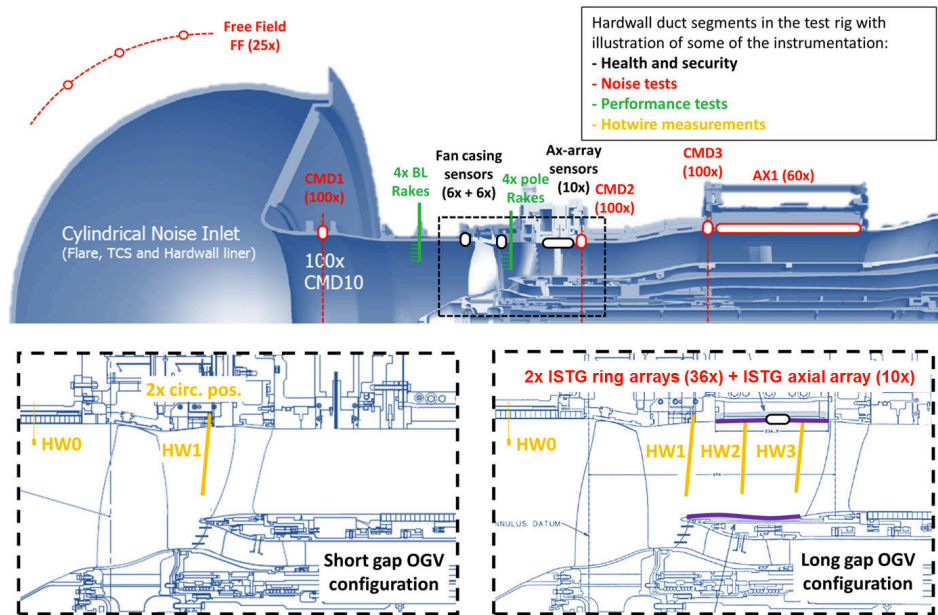


Figure 1 View of the UFFA fan rig of AneCom AeroTest. Ring arrays were used for acoustic measurements at the inlet (CMD1), interstage (ISTG) and bypass (CMD3) sections, and axial arrays at the interstage and in the bypass duct. Moreover, an array of 25 microphones, equally distributed from 0 to 120 degrees along an arc of radius 18.5 m centered on the fan axis at the nozzle inlet, was used for far field sound measurements upstream of the inlet.

In order to maintain the stage performance while reducing the vane count, the stator vanes are rescaled to keep the same solidity as the original OGV according to Rai *et al.* [14]. This modification consists in an axial rescaling (10% chord increase) and an azimuthal rescaling by the same factor. The leading-edge position remains the same in order to maintain the fan-OGV distance of the original configuration. The camber line and the thickness-to-chord ratio are also conserved. Determinant parameters for broadband noise predictions, such as sweep, lean and stagger angles, are also maintained. Since the vane count is modified, such a geometric transformation will have a significant impact on the tonal component of the noise but the Blade Passing Frequencies (BPF) will remain unchanged. However, it only has a limited impact on the broadband noise as shown by Leonard *et al.* [4] who performed a similar geometric transformation on the Source Diagnostic Test (SDT) configuration, and can be verified by the analytical models described hereafter.

The meridional view as well as a 3D view of the computational domain are depicted in Figs. 2 and 3.

The short inter-stage configuration is chosen. It consists of 20 fan blades and of 40 rescaled vanes. The fan tip gap is 0.78mm. The Inlet Guide Vanes (IGV) of the primary flow have been removed from the computational domain, since the broadband noise resulting from its interaction with the fan is considered as relatively negligible.

The computational domain extends from 4 fan axial chords upstream of the rotor at mid-span, to 6 vane axial chords downstream of the stator also at mid-span. Two main reasons led to choose these dimensions:

- They allow the boundary layers to develop on both the spinner and the casing upstream of the rotor.
- The core and bypass boundary conditions are easier to control especially regarding the reflection of sound waves .

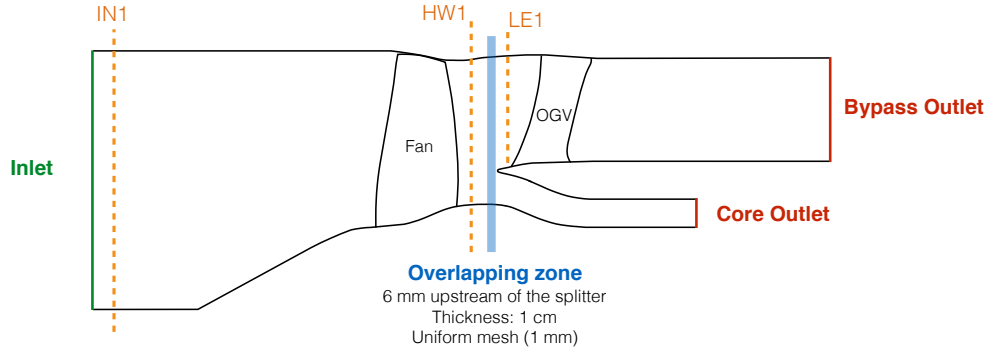


Figure 2 Computational domain. IN1, HW1 and LE1 correspond to the location of the axial cuts performed in the LES simulations. HW1 is also the location where the hot wire measurements have been performed.

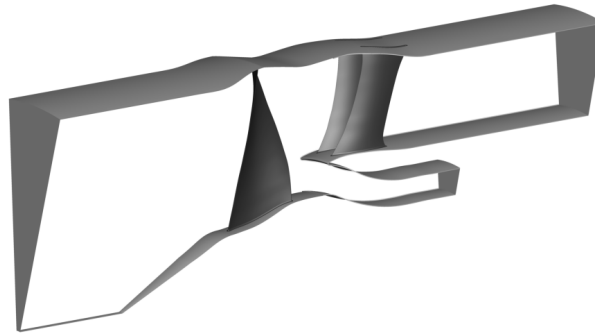


Figure 3 3D view of the computational domain.

B. Unstructured mesh

The mesh is a hybrid unstructured grid composed of 8 prism cells on walls, to accurately resolve the boundary layer, and of tetrahedral cells in the rest of the domain. Volume and surface refinements have also been introduced in order to ensure the quality of the mesh. Surface refinements have been mainly used to accurately discretize the blades and the vanes, especially the leading edges, the trailing edges and the fillets. This has resulted in a rotor mesh with more than 150 cells in the axial direction and 200 cells in the radial direction. For the stator domain, there are at least 100 cells in the axial direction and more than 150 in the radial direction. In the case of wall-modeled LES, the dimensionless wall distance to a surface in the normal direction (designated equivalently by y^+ or n^+), and in the tangential directions (s^+ for the streamwise direction and r^+ for the third local direction) have to meet certain requirements that are recalled in table 2 along with the wall-resolved LES requirements.

The n^+ values in the entire computational domain are shown in fig. 4. Figures 5 and 6 show a closer look at the n^+ , s^+ and r^+ values on the blade and vane skins, confirming that the mesh is consistent with the wall requirements for wall-modeled LES.

Four main volume refinement blocks have been used on both the fan and the OGV:

- Wake refinements to correctly transport the wakes down to the rotor-stator interface. This has guaranteed at least 15 points in the wake which ensures an accurate description of the physics.
- Leading-edge and trailing-edge refinements to ensure a smooth transition from the coarse to the fine mesh near the walls.
- Tip gap refinements: about 20 cells have been used to discretize this region.
- Inter-blade region refinements to guarantee a correct azimuthal description of the flow with at least 120 cells.

	Wall-resolved LES	Wall-modeled LES
s^+	50-150	100-600
r^+	10-40	100-300
n^+	1	30-150
Number of points in $0 < n^+ < 10$	3-5	-

Table 2 Wall mesh requirements for LES [15][16].

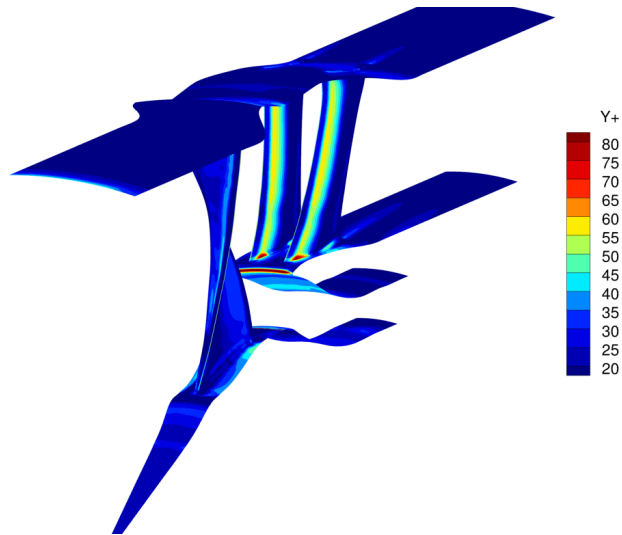
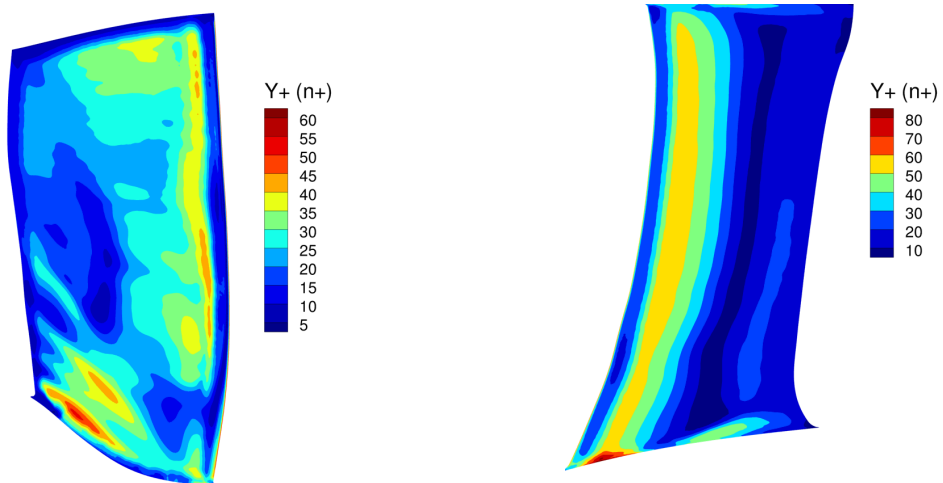


Figure 4 n^+ values.



(a) Rotor.

(b) Stator.

Figure 5 n^+ values on the rotor and stator suction sides

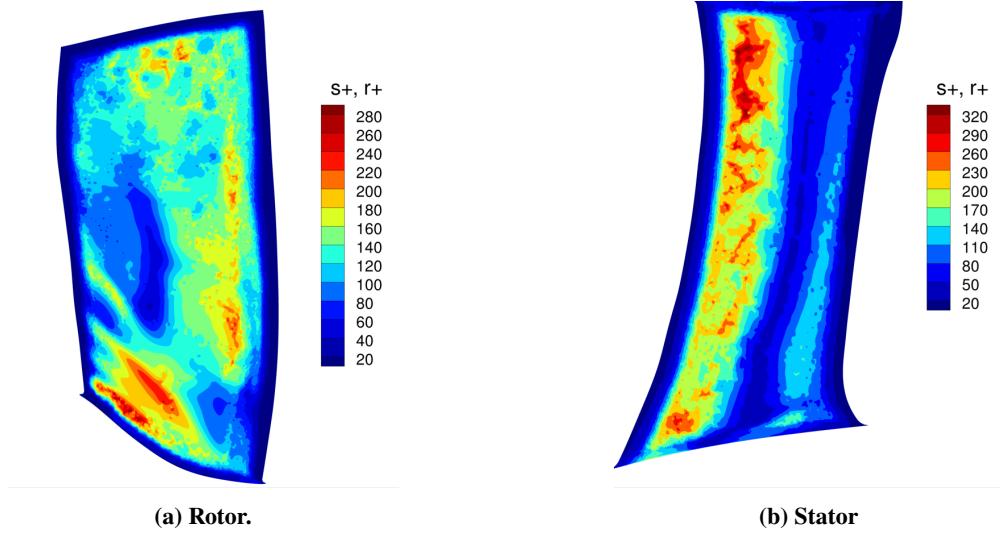


Figure 6 s^+ and r^+ values, rotor and stator suction sides.

The final mesh is displayed in Figs. 7, 8 and 9. These parameters eventually lead to a mesh composed of 55 million cells in the rotor domain and of 40 million cells in the stator domain. To avoid the unnecessary oversizing of the mesh observed on the RANS mesh [9], an optimized meshing approach based on the RANS velocity field of the wake has been used to create refinement blocks fitted to the wake, consequently reducing the CPU cost of the simulation. For this medium size mesh, a maximum cell size of 2 mm has been imposed so that acoustic waves up to 10 kHz (8 Blade Passing Frequencies (BPF)) are propagated with at least 25 points per wave-length. In terms of mesh quality the equivolume skewness has been maintained below 1, which guarantees that there are no degenerate cells. Similarly, the equiangle skewness is kept below 0.95, which is the limit to sliver cells.

C. Large Eddy Simulation

1. Solver and simulation specific features

The TurboAVBP code has been used to carry out the compressible LES on the ACAT1 configuration. This code consists in the external coupling of two LES simulations, the first one dedicated to the rotor, and the second one to the stator. Both computations are performed using the AVBP solver [17], which is developed by CERFACS and IFPEN. The two computational domains are coupled using an overset grid method, implemented in the code coupler openPALM, through which the data are exchanged between the two instances. The filtered compressible Navier-Stokes equations describing the mass, momentum and energy equations for a perfect gas are solved. Equations are solved using a finite-volume Lax-Wendroff time explicit scheme with second-order accuracy in time and space [18]. The Wall-Adapting Local Eddy-viscosity (WALE) subgrid-scale closure, developed by Nicoud and Ducros [19], is used to model the unresolved turbulent contributions. The inlet and outlets are treated using non-reflecting characteristics boundary conditions (NSCBC) [20]. At the inlet, the experimentally measured total temperature and pressure are imposed and the flow is purely axial with no turbulence injection [21]. At the outlet, the flow reaches a radial equilibrium which matches the mean static pressure extracted from a surface average of the static pressure at the outlet of the RANS simulation. Periodic boundaries are imposed on both lateral sides of the domain.

On all the solid walls, the boundary layer is modeled using a wall law inducing a no-slip condition at the walls (see the work of Nicoud *et al.* [22] for more details on the law itself). A linear law is imposed if the normalized wall distance satisfies the condition $y^+ < 11$, and a logarithmic law otherwise (Schmitt *et al.* [23]). In the present case, the mean y^+ is close to 35 which is a satisfactory value for wall-modeled LES [15].

The simulation has been initialized using the RANS solution of Lewis *et al.* [9] in order to reduce the transient period of the simulation. The time step for the simulation has been set to 3.7×10^{-5} ms to obtain around 22000 iterations

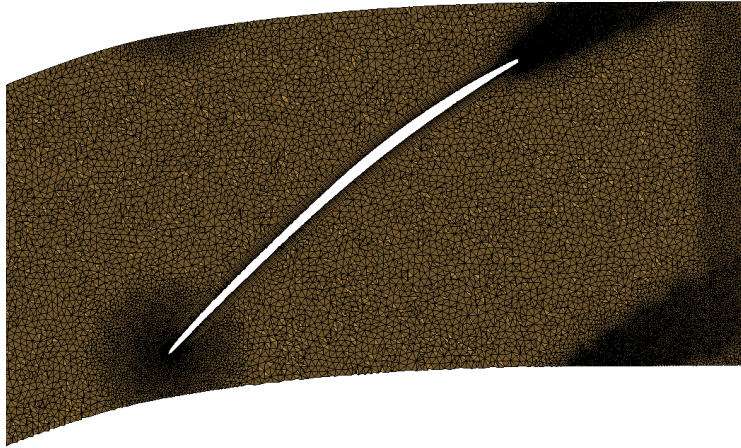


Figure 7 Midspan radial cut of the rotor domain mesh.

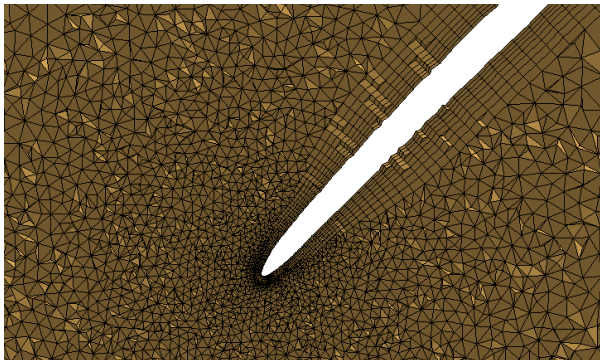


Figure 8 Rotor blade leading-edge mesh.

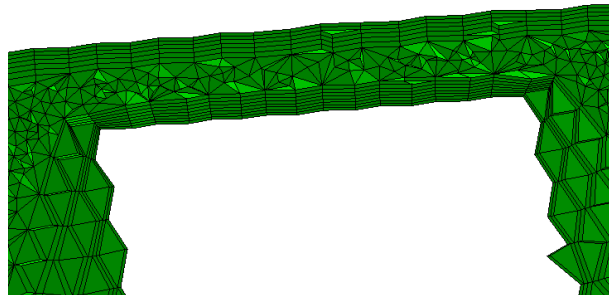


Figure 9 Rotor blade tip gap mesh.

per blade passage. The present numerical methodology has been validated on compressors [24], turbines [25] and turbofans [4, 26–28].

2. Convergence checking

The convergence state of the simulation has been checked by monitoring common integrated quantities (mass-flow rate at the inlet and outlets, pressure ratios in the bypass and core flows) as well as local quantities such as the pressure or the velocity using local control points (hereafter referred to as "probes"), the locations of which are indicated in Fig. 10. The stabilization of integrated quantities ensures the convergence of the mean flow. As was performed by Leonard *et al.* on the SDT configuration [4], the convergence of flow statistics was checked by analyzing the pressure signals retrieved from the probes with the method developed by Mockett *et al.* [29]. This method can be used to estimate the statistical error of a finite time signal and is particularly suited to identify the end of the transient regime of an LES. It has been applied to all the probes to estimate the best time to start recording the statistics of the actual simulation. The transient regime lasted around 5.5 rotations, and the statistics have already been recorded for about 4 rotations.

Over these 4 rotations, the wall pressure fluctuations on the rotor blades and the stator vanes have been recorded as well as the pressure and the velocity components at the three axial positions shown in Fig. 2 (IN1, HW1 and LE1) in order to be post-processed. These flow extractions have been performed every 250 time steps, which corresponds to a sampling rate of about 110 kHz.

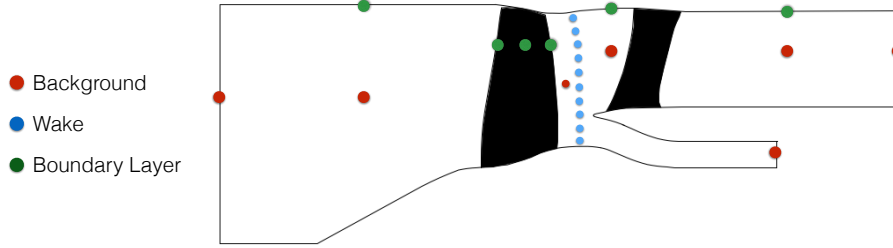


Figure 10 Probe locations.

V. Aerodynamic analysis

The results obtained from the LES are presented in the following sections. Results are compared to both the experimental performance parameters and the hot-wire measurements.

A. Global performance

Tables 3 and 4 summarize the performance parameters at approach condition obtained from the LES. These values were obtained from a mass-flow rate weighted average over an axial field cut at the splitter location, upstream of the stator. The agreement of the LES results with the experimental data is excellent, showing negligible discrepancies for both the mass-flow rates and the pressure ratios.

	Massflow rate (kg/s)		
	Bypass	Core	Total
Experiment	48.745	6.411	55.156
RANS	48.745	6.411	55.156
LES	48.787 (+0.09%)	6.395 (-0.25%)	55.186 (+0.05%)

Table 3 Mass-flow rates obtained at approach condition.

	Fan pressure ratio		
	Bypass	Core	Total
Experiment	1.110	1.100	1.109
RANS	1.106 (-0.36%)	1.098 (-0.2%)	1.105 (-0.36%)
LES	1.106 (-0.36%)	1.095 (-0.45%)	1.105 (-0.36%)

Table 4 Fan pressure ratios obtained at approach condition.

B. Mean flow

1. Friction line analysis

As the flow speed is reduced at approach condition with respect to cruise condition, higher angles of attack can be observed at the fan leading edge, which generally results in local flow separations. In order to identify these detached zones, the mean axial component of the wall shear on the suction side of the blades and vanes is displayed in Figs. 11 and 12 respectively. As expected, a leading-edge flow separation appears from 20% of the fan span up to the tip of the

rotor. The flow reattaches before reaching a quarter of the blade chord and remains attached down to the trailing-edge on most of the fan span. Between 30% and 60% of the rotor span however, a large flow detachment occurs from 60% of the axial chord down to the trailing edge. Regarding the vane, the flow remains attached until it reaches half of the vane chord where a flow detachment covering almost all the vane span occurs. This flow separation was not predicted by the RANS simulation [9]. Between 20% and 95% of the vane span, the flow reattaches before reaching the trailing edge while under 20% it remains detached.

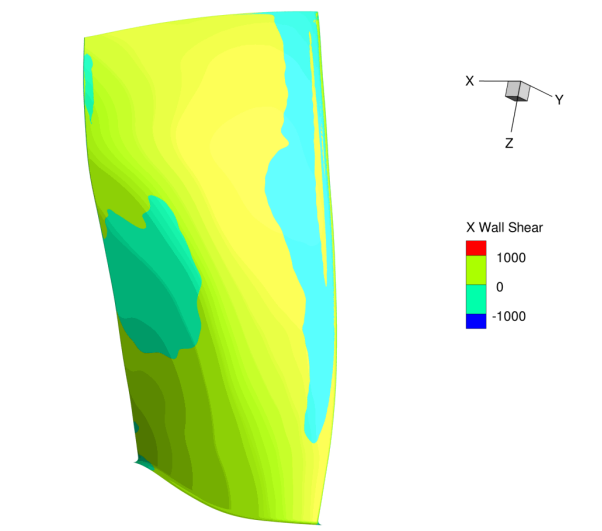


Figure 11 Axial component of the wall shear on the blade suction side.

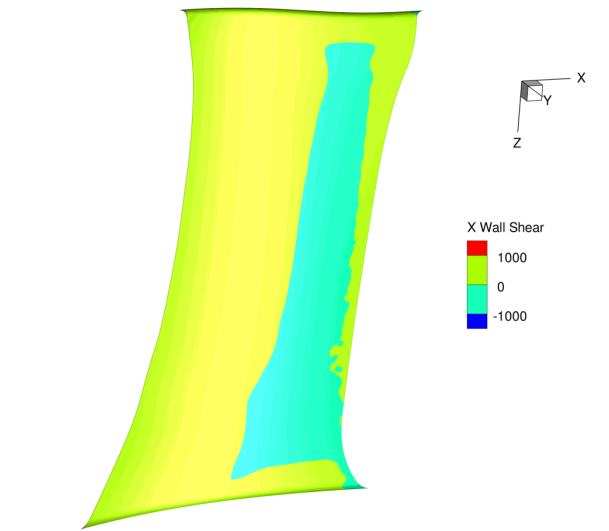


Figure 12 Axial component of the wall shear on the vane suction side.

2. Fan wake analysis

Broadband interaction noise directly depends on the turbulent state of the flow impacting the stator row. As a consequence, typical turbulence variables such as the turbulence kinetic energy (TKE) within and outside of the wakes, and the flow characteristic dimensions (wake width, integral length scale) are usually prescribed as input parameters for analytical models. They notably have a substantial effect on the subsequent noise predictions [30]. An accurate simulation of these flow characteristics is then compulsory to ensure the reliability of the noise predictions, whether numerical or analytical.

With the aim of checking the reliability of the present simulation, Figures 13-16 compare the three velocity components and the TKE from both HW measurements and LES at the hot-wire HW1 location ($X=-2.685\text{m}$, see Fig. 2).

The axial velocity (Fig. 13) is in very good agreement with the experimental data. The wake tilting is well recovered by the LES, as was already observed in previous simulations on the SDT [4, 26, 31]. The casing boundary layer is thicker in the LES and part of the tip gap vortex is not well captured in comparison with the experiment. A finer mesh may be needed in this flow region to better capture this flow feature. A slight overestimation, which is within the experimental uncertainty, can be observed in the background flow over the whole blade span. The wake velocity deficit is slightly less important in the LES, especially near the tip of the rotor where the velocity deficit notably decreases, which is not observed in the HW measurements. It should be underlined at this point that the experimental wakes vary from one blade to another, a few blades shedding particularly thick wakes (e.g. 4 o'clock blade). The computation assumes a perfect axisymmetry that should be ideally obtained in the experiment. Similarly the hotwire measurements are questionable in the gap region where the flow is expected to exhibit intense swirl that is likely to flaw the HW measurements.

The azimuthal velocity (Fig. 14) is in very good agreement with the experimental data. A slight overestimation is observed in the core flow, which could be partly explained by the absence of the IGV in the LES setup.

The radial velocity (Fig. 15) is the velocity component which shows the largest discrepancies. This component is well captured in the wake and in the upper part of the background flow. However, a substantial overestimation is observed close to the casing and in the core flow. This might be partially explained by the lack of accuracy of the experimental estimate using hot wires since comparable discrepancies have been observed on other configurations [32]. The radial velocity is indeed very small compared to the 2 other components: therefore slight differences in the main components account for relatively large variations of the radial velocity.

Finally, the turbulence kinetic energy (Fig. 16) is significantly overestimated by the LES. This might be caused by the significant flow detachment observed at the rotor leading edge, which might be more important in the simulation than in the experiment. This flow separation may indeed induce high levels of TKE close to the rotor suction side which then interact with the wakes. As already mentioned for the axial component, it should be pointed out that HW measurements show significant wake-to-wake variations that limit their trustworthiness and cannot be reproduced by the simulation. Furthermore, studies on the same case by François *et al.* [33] and by Polacsek *et al.* [34] have shown similar discrepancies with the experimental data using a ZDES approach with a 380 million cell mesh, unveiling a potential lack of accuracy of the HW measurements. The overall agreement of the LES with the experiment is still quite satisfactory. Nevertheless, such an overestimation of the turbulent kinetic energy suggests the need for a finer wall mesh to capture more precisely the leading edge flow detachment, or at least to check the reliability of the present computation. Similarly to the RANS simulation [9], this overestimation of the TKE may be detrimental to the noise prediction but has also led to interesting outcomes, as shown in the following sections.

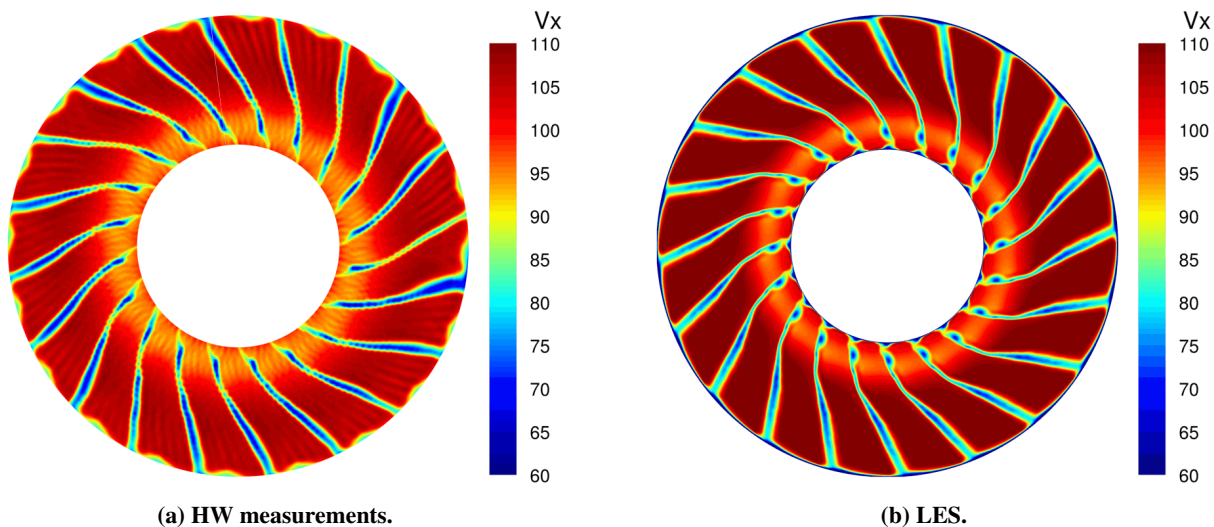


Figure 13 Axial velocity field at position HW1.

VI. Broadband noise predictions using analytical models

This section presents the LES-informed analytical predictions that have been performed. The objective is to assess the impact on the noise predictions of the use of the more accurate LES input parameters, with respect to the RANS-informed predictions performed previously [9].

A. Extraction of input data for acoustic models

Analytical models require several input parameters in order to reconstruct the stator incident flow and compute the resulting loading fluctuations:

- The axial velocity
- The absolute velocity
- The turbulence intensity (TI) in the wake and the background flow

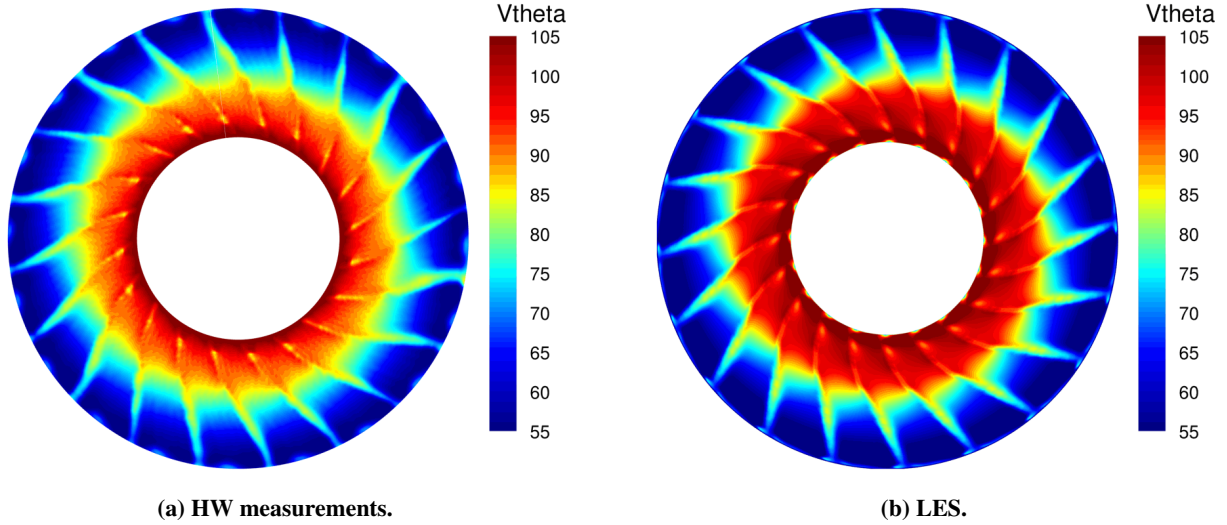


Figure 14 Circumferential velocity field at position HW1.

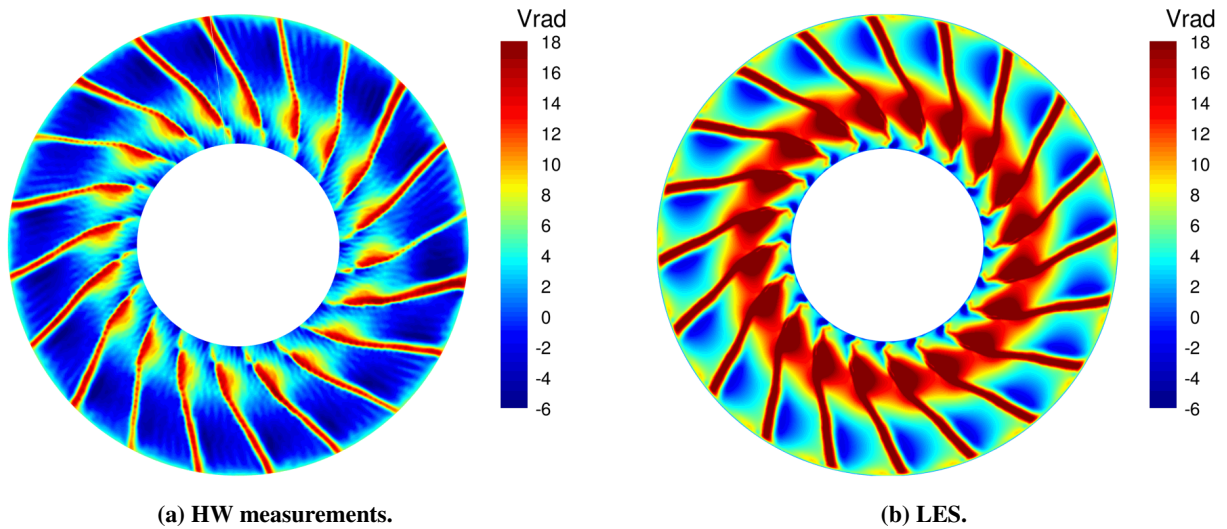


Figure 15 Radial velocity field at position HW1.

- The turbulence integral length scale (TLS) in the wake and the background flow
- The wake half width

These flow parameters have been retrieved from the LES thanks to an axial cut located at the LE1 position (see Fig. 2). This cut has been performed as close as possible to the stator leading edge in order to get a representative description of the flow that is actually interacting with the vane cascade. A well adapted and fairly accurate way to extract these parameters is to assume a Gaussian shape for the wake, based whether on the absolute velocity deficit or on the turbulence kinetic energy (TKE). Performing a Gaussian fit on the extracted wakes then enables to separate the background flow from the wake variables by applying a 20% threshold (see Fig. 17).

Multiple processes for estimating the streamwise turbulence lengthscale based on numerical simulations are available. For RANS simulations, the first one, proposed by Pope [35], makes direct use of the turbulent variables k and ω through the following relationship:

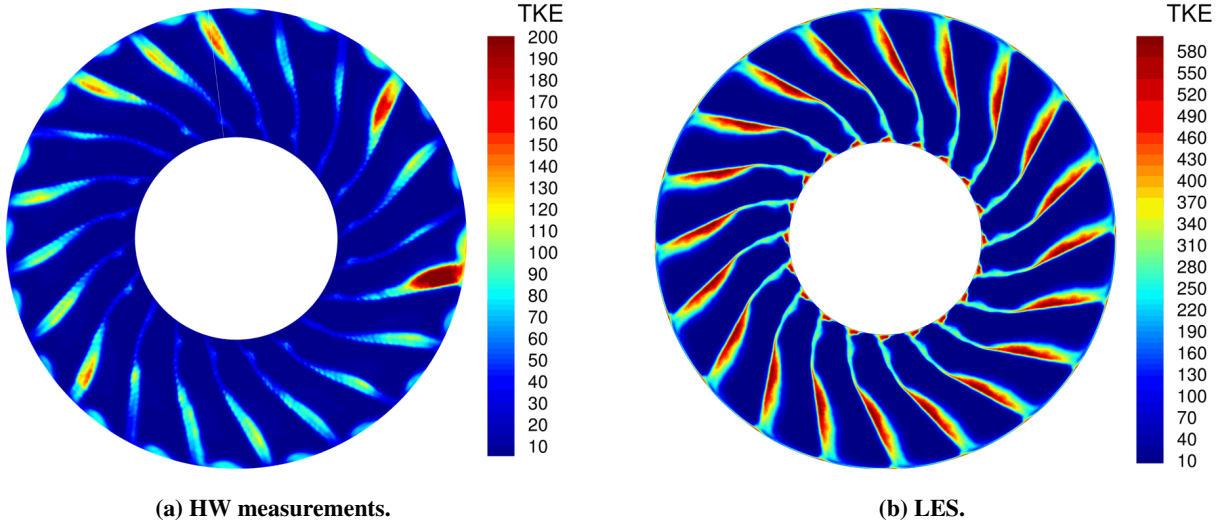


Figure 16 Turbulence Kinetic Energy at position HW1 (with different color map scales for improved legibility)

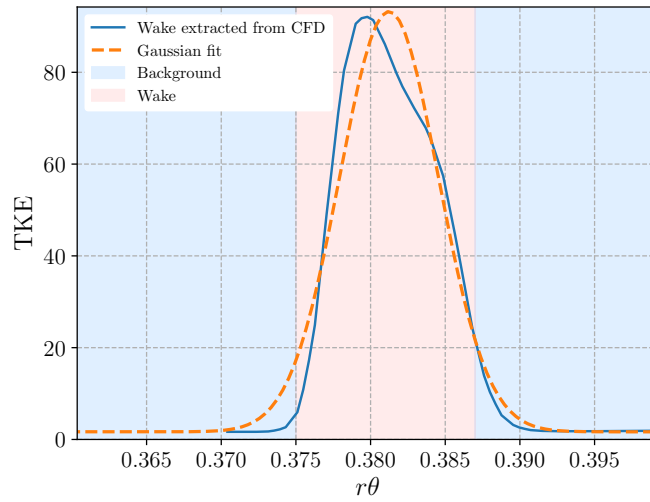


Figure 17 Wake extraction using a Gaussian fit.

$$\Lambda_p = 0.43 \frac{\sqrt{k}}{C_\mu \omega} \quad (1)$$

with $C_\mu = 0.09$. Another estimate can be obtained using the wake width L_w with the empirical relationship of Jurdic *et al.* [36]:

$$\Lambda_j = 0.21 L_w \quad (2)$$

For the latter relationship, the wake and background TLS are the same. This estimate can obviously be used also when retrieving data from LES. Another integral length scale estimate can be obtained using the unsteady data extracted from

the temporal recording made on an axial cut through the computation of the temporal autocorrelation function:

$$R_{uu}(\mathbf{x}, \tau) = \frac{\overline{u'(\mathbf{x}, t)u'(\mathbf{x}, t + \tau)}}{u_{RMS}'^2(\mathbf{x})}, \quad (3)$$

where $u'(\mathbf{x}, t)$ is the axial velocity fluctuation at position \mathbf{x} and time t , and $u_{RMS}'(\mathbf{x})$ the root mean square of the velocity fluctuations at position \mathbf{x} . The autocorrelation can then be used to compute the temporal integral scale [35]:

$$\Lambda_t = \int_{\tau=0}^{\infty} R_{uu}(\mathbf{x}, \tau) d\tau. \quad (4)$$

Under Taylor's frozen turbulence assumption [35, 36], an integral length scale can finally be computed as follows:

$$\Lambda_c = \bar{U}\Lambda_t, \quad (5)$$

where \bar{U} is the mean axial velocity transporting the turbulence.

In order to compute the TLS from the LES using Λ_j , a phase locked average has been performed over about 4 rotations on the axial cut upstream of the OGV leading edge at the LE1 position (see Fig. 18). The Λ_c estimate was also computed on the same axial cut and over the same simulation time. The latter estimate was performed using the same approach as Odier *et al.* [28].

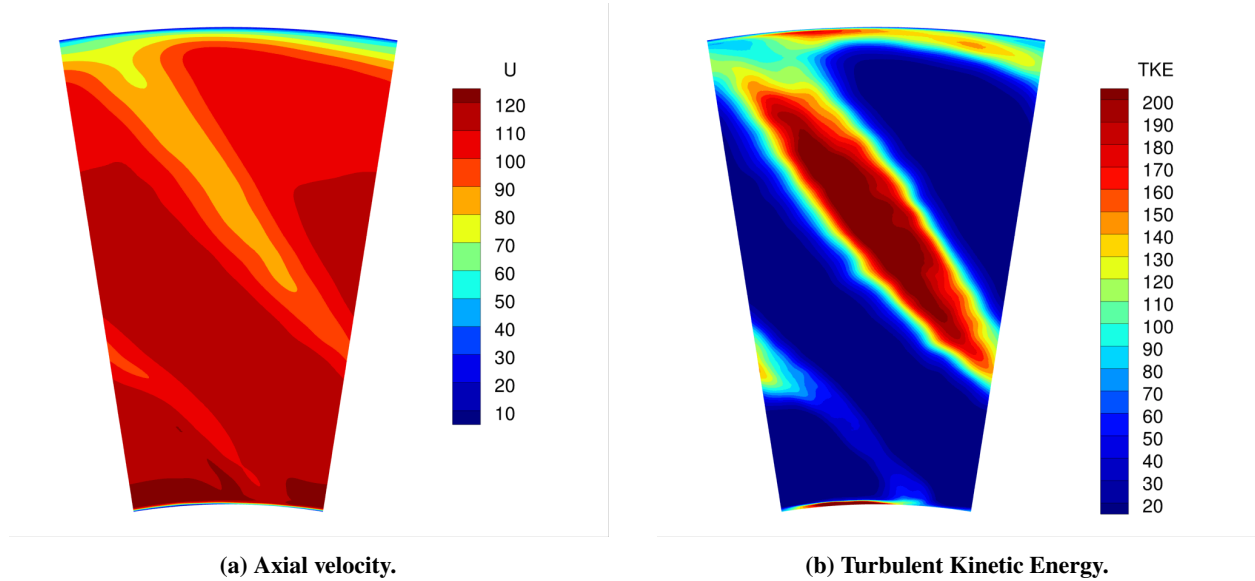


Figure 18 Phase locked average at LE1 position.

Figures 19 and 20 show the radial evolution of the input parameters resulting from the previously explained extraction processes. The LES values are plotted along with the RANS extractions that were performed by Lewis *et al.* [9] for the same case. It should be noted that the RANS flow was first extrapolated from the rotor domain down to the stator trailing edge, using Jaron's method [37], in order to get a realistic flow at the stator leading edge in spite of using a mixing plane approach. Nevertheless, since the distance between the leading edge and the axial cut of the LES is relatively small, the flow disparities between these two positions are expected to be relatively small as well, which ensures a reliable comparison between the two extractions.

The absolute and axial velocities (Figs. 19a and 19b respectively) extracted from the LES and the RANS are relatively similar, with values that are slightly higher at the stator midspan for the RANS. The turbulence intensity (TI), however, shows significant disparities. On the one hand, the background TI (Fig. 19c) of the LES is slightly lower than for the RANS. This may be due to the fact that no turbulence has been prescribed at the inlet of the LES, whereas an inlet

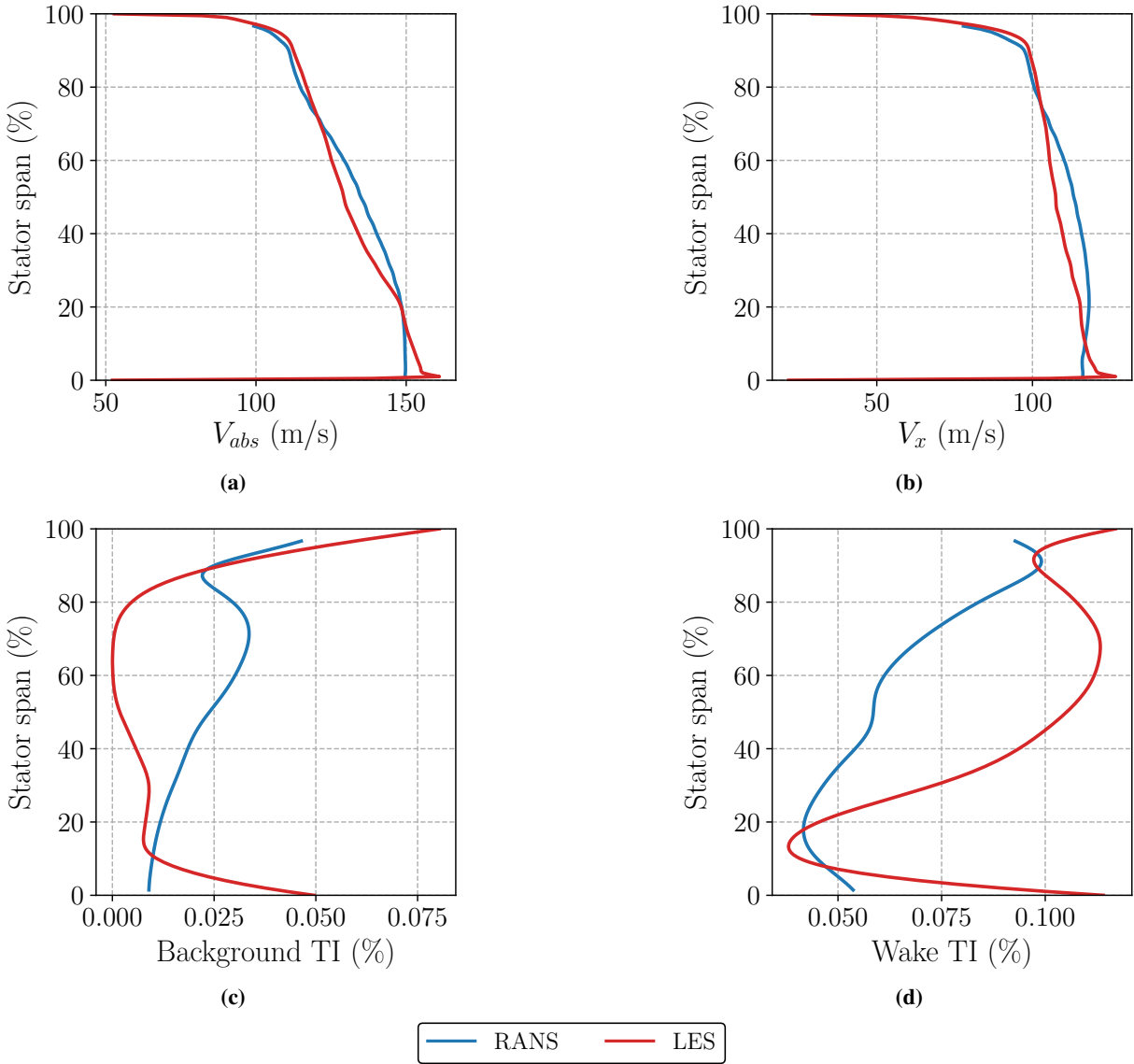


Figure 19 Comparison of the model input parameters extracted from both RANS and LES.

turbulence intensity of 0.03% has been imposed in the RANS. On the other hand, the wake TI is higher in the case of the LES and can reach values up to twice the RANS wake TI between 15% and 80% of the stator span (Fig. 19d). This may be explained by the flow separation at the fan leading edge that is more significant in the LES than in the RANS, and interacts with the downstream wake, contributing to its thickening. The tip gap region is characterized by a decrease and a sudden increase in the TI, showing the interaction of the wake and the tip gap flow. For both background and wake TI, the LES unveils a sudden increase in TI near the hub and the casing. However, in the case of the RANS, this increase cannot be observed at the hub because the extrapolation process does not account for the presence of the splitter.

The different TLS estimates are plotted in Fig. 20. The radial evolution of Λ_j is very similar for both simulations, except at 15% of the stator span where a slight decrease in the TLS, which may result from the interaction of the wake with the splitter, is observed for the LES. The values are higher for the LES since the wake width is larger than in the RANS over the whole vane span. Once again, this may be the consequence of a more substantial interaction between the

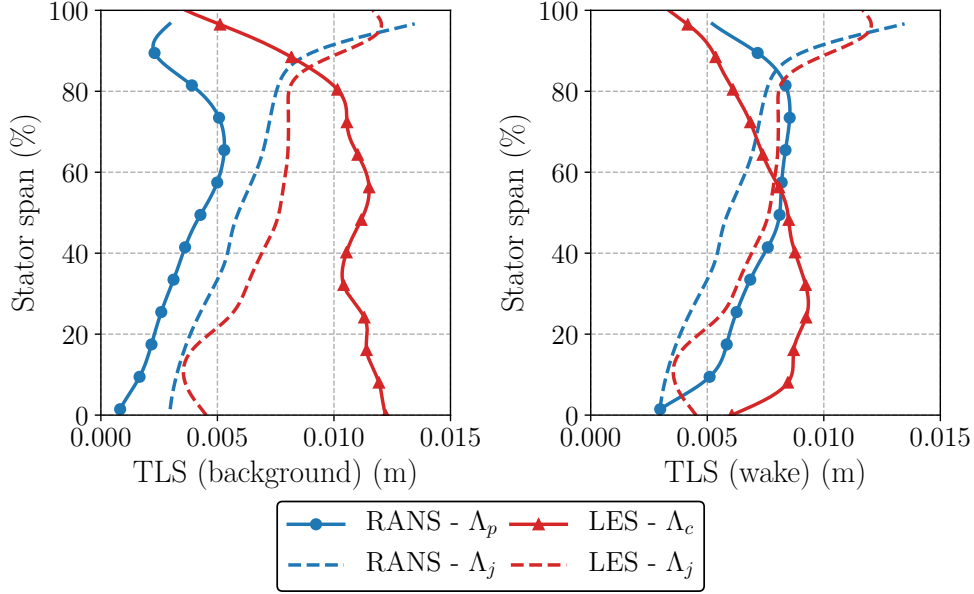


Figure 20 Comparison of the different TLS estimates extracted from both RANS [9] and LES.

separated flow and the downstream wake in the LES. The same increase in Λ_j is observed near the tip gap region where the wake substantially thickens because of its interaction with the tip gap flow, which is certainly not well captured by the RANS prediction as it is highly unsteady.

The Λ_c estimate displays a quite different behavior than the Λ_j . In the background flow, Λ_c is almost constant from the hub up to 80% of the vane span with significantly larger values than those obtained for Λ_j . Near the tip, its shape is similar to the Λ_p estimate for the RANS, with a decrease in the estimated TLS as one gets closer to the casing. Similar observations were made by Leonard *et al.* on the SDT configuration [4]. In the wake, the Λ_c estimate provides values that are of the same order of magnitude as the Λ_j estimate. However, the radial evolution of Λ_c displays pronounced differences with Jurdic's estimate. Λ_c increases from the hub up to 40% of the vane span and then decreases up to the casing. The decrease in Λ_c in the wake starts closer to the hub than in the background flow. The wake TLS is smaller than that in the background, which is consistent with the real physical behavior of the flow. This behavior is for instance not well reproduced by the Λ_p estimate for which the TLS is slightly larger in the wake.

The results obtained from Λ_c question the validity of Jurdic's estimate in such a flow configuration. It seems that the flow detachment observed on the fan leading edge has significantly modified the wake structure and has led to a flow configuration that does not correspond to the one in which this estimate was observed. This result may also indicate that a finer mesh is needed in the background flow or on the blade surface, to faithfully capture the turbulent structures.

B. Analytical model results

Two models representing the state of the art of analytical broadband RSI noise prediction have been applied: the model of Hanson [38], and the model of Posson [5, 39, 40] as implemented in the *Optibru* platform. They are both derived from Glegg's model [41] which computes the acoustic field resulting from the interaction of a 3D incident gust with a rectilinear cascade of zero-thickness flat plates of infinite span. To account for the spanwise geometric and aerodynamic variations, they rely on the strip theory in which the stator is divided into several unwrapped radial strips, each of them corresponding to Glegg's configuration.

The main difference between the two models is the acoustic propagation method. On the one hand, Hanson's model propagates the acoustic waves within each strip and accounts for the mean axial flow. On the other hand, Posson's model computes the vane unsteady loading which is then used as an equivalent dipole source within an in-duct acoustic analogy that takes into account a uniform axial flow. Consequently, Posson's model considers a distribution of the

acoustic energy over the duct cut-on modes, whereas Hanson's model totally neglects the duct propagation effects.

The experimental sound power level (SWL) displayed in the following result comparisons have been computed using microphone measurements. The upstream SWL obtained from the forward arc was computed by integrating the sound pressure spectra measured by the far-field microphones weighted by the sine of the radiation angle. The downstream SWL was computed using the pressure signals at the casing of the bypass section by assuming a particular energy distribution over the acoustic cut-on modes. This method is referred to as Wave Number Decomposition (WND) and is detailed in Tapken *et al.* [12].

Both models were informed with the input parameters described in the previous section. Figs. 21 and 22 show the prediction for both noise models using the previously discussed integral length scale estimates. The LES results have been plotted along with the RANS predictions performed by Lewis *et al.* [9] to get a more comprehensive analysis. Regarding the LES-informed predictions, the integral length scale estimate has a significant impact on the noise predictions for both models. Similarly to what was observed by Lewis *et al.* [9] and by Kissner *et al.* [42] for the RANS-informed predictions, the fact that Λ_j is larger than Λ_c near the casing leads to higher noise levels at low frequencies, confirming that the strips located near the casing are responsible for a significant part of the radiated noise. It should however be noted that the gap at low frequency between the Λ_c and Λ_j predictions is several dB lower than between the Λ_p and Λ_j RANS-informed predictions, despite similar trends in the near-casing region. This may be due to the high Λ_c values in the lower part of the background flow that could counter-balance the effect of the near-casing strips. Moreover, the near casing gap between Λ_c and Λ_j is substantially smaller than the one observed between the two TLS estimates used for the RANS. This behavior has eventually led to a maximum low-frequency gap of 2 dB for Hanson's model and 3 dB for Posson's model between the two LES predictions. It emphasizes the paramount role of the tip flow wake, confirming the relevance of carrying out well resolved unsteady simulations such as LES in that region.

Despite noticeable disparities in the TLS estimates, especially in the background flow, the LES-informed predictions using the two estimates almost overlay above 5kHz. This is particularly the case for Hanson's model. For Posson's model, the TLS disparities have had a slight impact at high-frequencies as well. Indeed, in addition to the near-casing strip effect, the TLS differences has induced a slight tilting of the spectrum, leading to an almost constant 1 dB gap above 5 kHz between the two LES predictions.

Considering only the predictions using Λ_j , it appears that the LES predictions are closer to the experimental data than the RANS-informed predictions. Similar observations were made by Leonard *et al.* [4] on the SDT configuration when comparing the TLS estimate impact on both RANS and LES-informed analytical models. In the present case, an increase in the SWL by 2-3 dB is observed over the whole frequency range for the LES with respect to the RANS data. This increase results from the simultaneous increase in Λ_j and in the wake TI for the LES relatively to the RANS.

Figure 23 shows the direct comparison of the LES-informed predictions obtained from Hanson's and Posson's models, when using the two available TLS estimates. As for the RANS, Posson's model tends to underestimate the noise at low frequency relatively to Hanson's model. This is mainly attributed to the duct cut-off effect which has a noticeable impact, especially at low frequencies for which a major part of the first modes is cut-off. The frequency for which the maximum SWL is observed is well captured by the model of Posson for both upstream and downstream predictions when using Λ_j . Hanson's model, however, only captures the frequency of the SWL peak for the upstream prediction. When using Λ_c , the capacity to capture the frequency at the SWL peak is conserved by both models. In terms of shape, Hanson's model is closer to the upstream experimental spectrum whereas Posson's model recovers quite faithfully the shape of the downstream experimental spectrum. This may due to the fact that Posson's model uses the inner and outer radii of the bypass section as references for the in-duct propagation, leading to a more important cut-off effect for the upstream part but to a more faithful downstream prediction. In terms of absolute levels, both models underestimate the upstream noise from medium to high frequencies, with a gap ranging from 2 to 10 dB for the highest frequencies. For the downstream prediction, Hanson's model recovers the experimental noise level whereas an underestimation by 2 to 5 dB is observed for Posson's model over the whole frequency range.

As already discussed in [9], Hanson's model provides an overall better estimate of the intake and exhaust sound power levels than Posson's model. Conclusions have to be drawn carefully since the duct geometry both upstream and downstream of the OGV, as well as rotor reflections are likely to impact the sound transmission. In that perspective, Posson's model better takes into account the transmission across the stator and the downstream duct that is cylindrical, since it expresses the solution as a sum of cut-on cylindrical duct modes. As a consequence, the seeming under-prediction of Posson's model may actually be the most trustworthy for the RSI mechanism, which would indicate the presence of

other non-negligible noise sources in the actual experiment. The flow detachment on the rotor leading edge, for instance, might be an interesting additional source to consider in future studies. The fact that both models still under-predict the radiated noise in spite of the fact that the TI levels are significantly higher in the LES than in the experiment also supports this latter point.

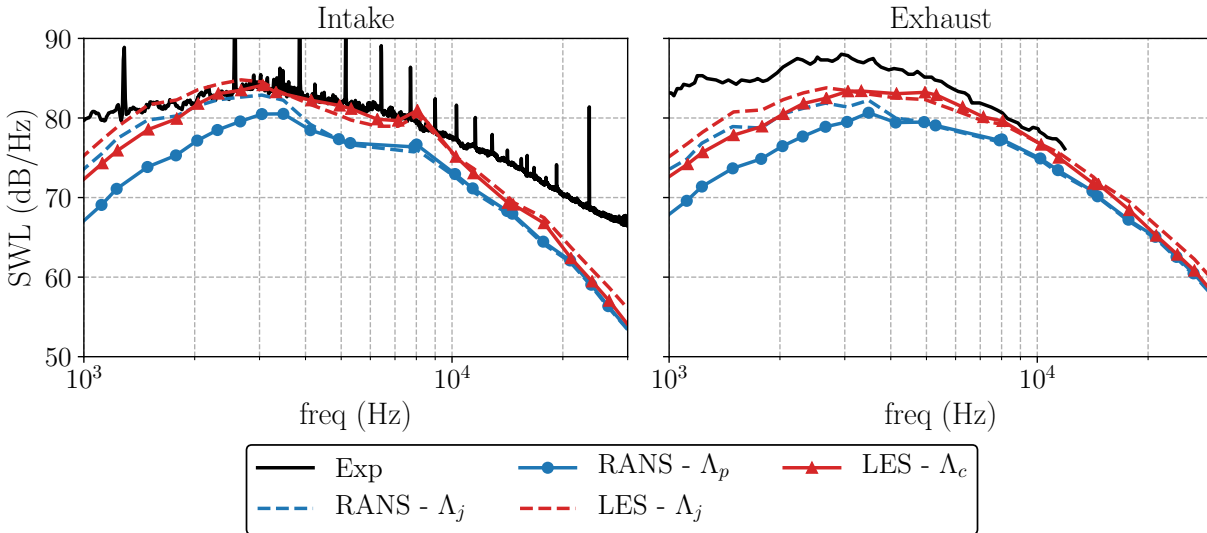


Figure 21 Upstream SWL (left) and Downstream SWL (right) spectra predicted by Posson's model.

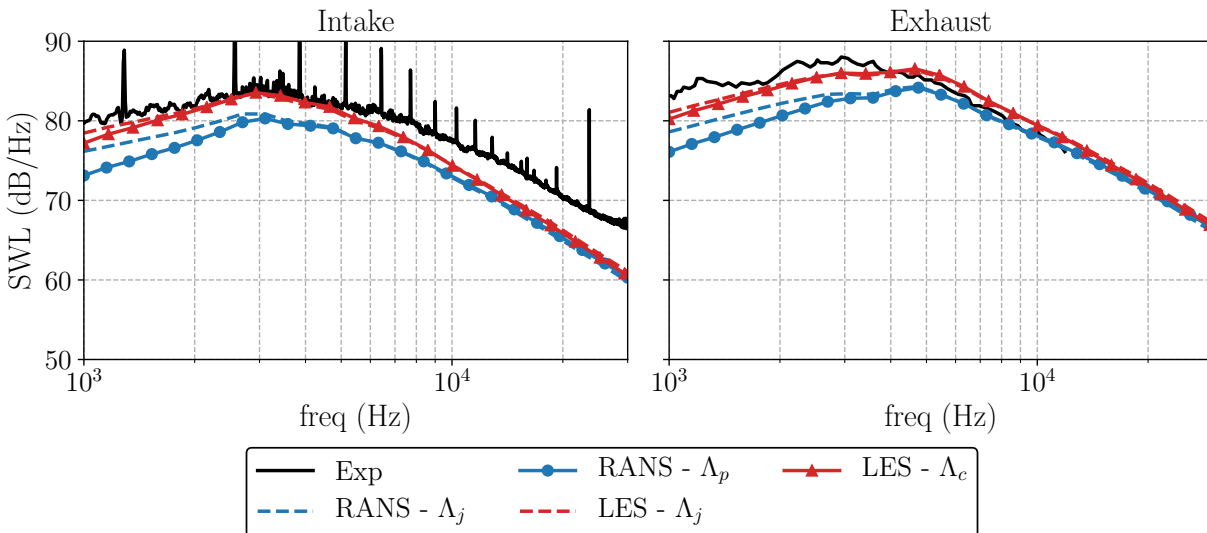


Figure 22 Upstream SWL (left) and Downstream SWL (right) spectra predicted by Hanson's model.

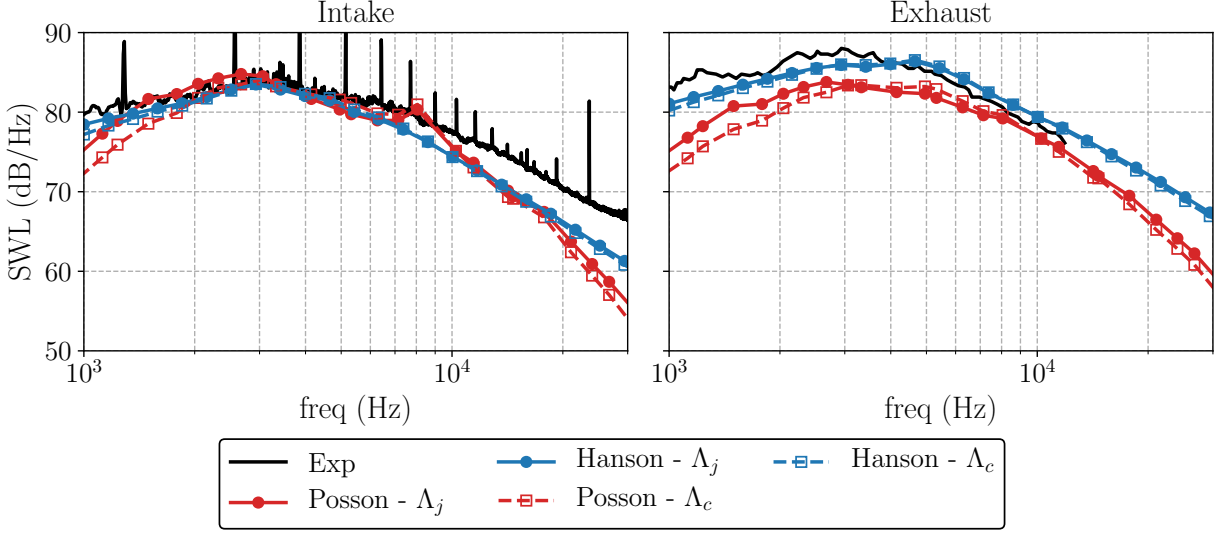


Figure 23 Upstream SWL (left) and Downstream SWL (right) spectra predicted by Hanson's and Posson's models using LES data.

VII. Broadband noise predictions using a hybrid numerical approach

The previous LES-informed analytical model approach has been performed for comparison purposes but does not represent a viable noise prediction approach given the cost of an LES. LES is in fact better suited for high-order numerical hybrid methods dedicated to broadband noise predictions. This kind of method is a two-step approach that decouples the computation of the acoustic sources, performed through a scale-resolving simulation such as LES, from the propagation, usually performed through the use of an acoustic analogy. In the present case, the sources correspond to the wall pressure fluctuations on the stator surface, which have been extracted from the simulation over about 4 rotations. These pressure fluctuations have then been used as dipole sources within the Ffowcs Williams and Hawkins (FW-H) free-field analogy, as implemented in the tool *SherFWH* developed by the Aeroacoustics Group of Université de Sherbrooke [43]. *SherFWH* corresponds to an implementation of the formulations of Casalino [44] and Najafi-Yazdi *et al.* [45]. As previously mentioned, FW-H's analogy propagates the sound in the free-field, which means that the duct geometry is neglected. Moreover, extracting the sources directly on the vane surface implies that the quadrupole sources, related to the volume term of the FW-H analogy [46], is neglected. This is actually a fairly reasonable assumption since the tip relative Mach number of the rotor is of 0.57, which makes it possible to neglect both monopole and quadrupole sources [46].

The pressure fluctuations on the vane have been recorded over almost 4 rotations with a sampling frequency of 110 kHz, leading to a Nyquist frequency of 55 kHz. Considering that 25 points per wavelength are required to resolve an acoustic wave, the vane surface mesh parameters lead to an acoustic cut-off frequency of 116 kHz. The far-field SWL has been obtained using Welch's method and Hann windows with 50% overlap. The impact of the number of windows on the frequency resolution Δf of the signal is presented in Table 5.

Number of averages	3	10
Δf (Hz) - 50% overlap	84	282
Δf (Hz) - no overlap	42	141

Table 5 Impact of the number of windows and of the overlap on the signal post-processing.

Figures 24 and 25 show the results obtained using 3 and 10 windows respectively for a better readability. The noise

prediction obtained using the pressure fluctuations on the entire vane surface is plotted in blue. For both upstream and downstream predictions, the FW-H prediction recovers quite faithfully the overall shape of the experimental spectrum. In terms of absolute levels, however, a significant overprediction of the radiated noise can be observed. This is especially the case for the upstream prediction that displays a 10 dB gap from low to medium frequencies. Above 6 kHz, however, this gap decreases to 5 dB and remains constant up to higher frequencies. The first BPF harmonics are recovered with an overprediction of 10 dB for the BPF, while the second harmonic is slightly under-predicted (-2 dB) and the third one is well captured. The higher harmonics, however, are not well recovered by the method. These discrepancies regarding the tonal noise are expected since the vane count has been modified to reduce the computational domain. The overprediction of the noise for the downstream part is not as important as for the upstream one. The difference with respect to the experiment is only of 2 dB on most of studied frequency range, except at low frequencies where it can reach 5 dB. This overall overprediction may be attributed to the fact that the FW-H analogy only considers a free-field propagation, which neglects the duct cut-off effect as well as the real distribution of the acoustic energy over the duct modes. As shown by Pérez *et al.* [27], the use of Goldstein’s analogy [8], which takes into account these duct specific features, could lead to a 5 to 10 dB reduction of the predicted noise over the whole frequency range with respect to the FW-H based prediction. Furthermore, as mentioned in Section V.B.1, a flow detachment occurs in the rear part of the stator vane, which was not observed in the RANS study. This flow separation, if not well predicted, may be partly responsible for the observed overprediction. In order to assess how significant its contribution to the radiated noise is, the vane has been split in two parts: the front part, consisting of the first 40% of the vane axial chord over the entire vane span, and the aft part, which consists in the 60% left. Considering this splitting, the power spectral density (PSD) Γ_{full} induced by the pressure fluctuations on the full blade at a particular observer point can be rewritten as follows:

$$\Gamma_{full} = \Gamma_{Front} + \Gamma_{Aft} + 2Re(\Gamma_{Front,Aft}), \quad (6)$$

where Γ_{Front} and Γ_{aft} are the PSD induced by the front and the aft parts of the vane respectively, $\Gamma_{Front,Aft}$ is the cross-spectral density between the front and the aft signals (corresponding to the Fourier transform of the cross-correlation function), and $Re()$ denotes the real part of the quantity in parentheses. These three terms (Γ_{Front} , Γ_{Aft} , and $2Re(\Gamma_{Front,Aft})$) have been plotted along with the full-vane based prediction in Figs. 24 and 25.

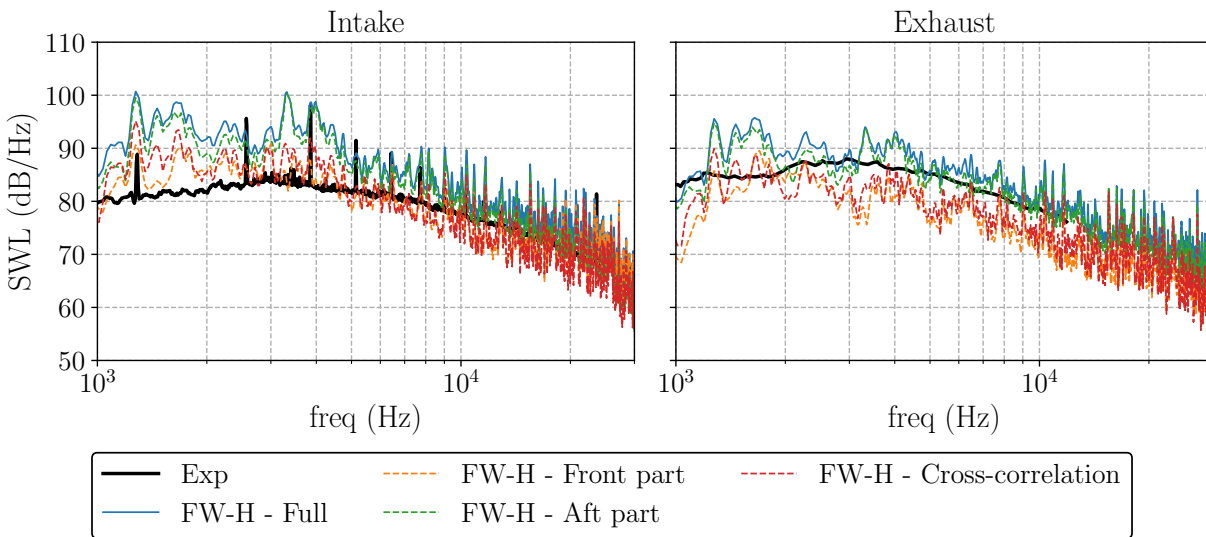


Figure 24 Upstream SWL (left) and Downstream SWL (right) spectra obtained from Ffowcs Williams and Hawkings analogy (3 windows).

As it can be seen, the aft part of the vane is responsible for most of the noise radiated by the vane, which means that in the present computation, the noise due to the flow separation may be more important than expected. Moreover, the fact that the front and the cross terms display noise levels similar to, or lower than those observed in the experiment may

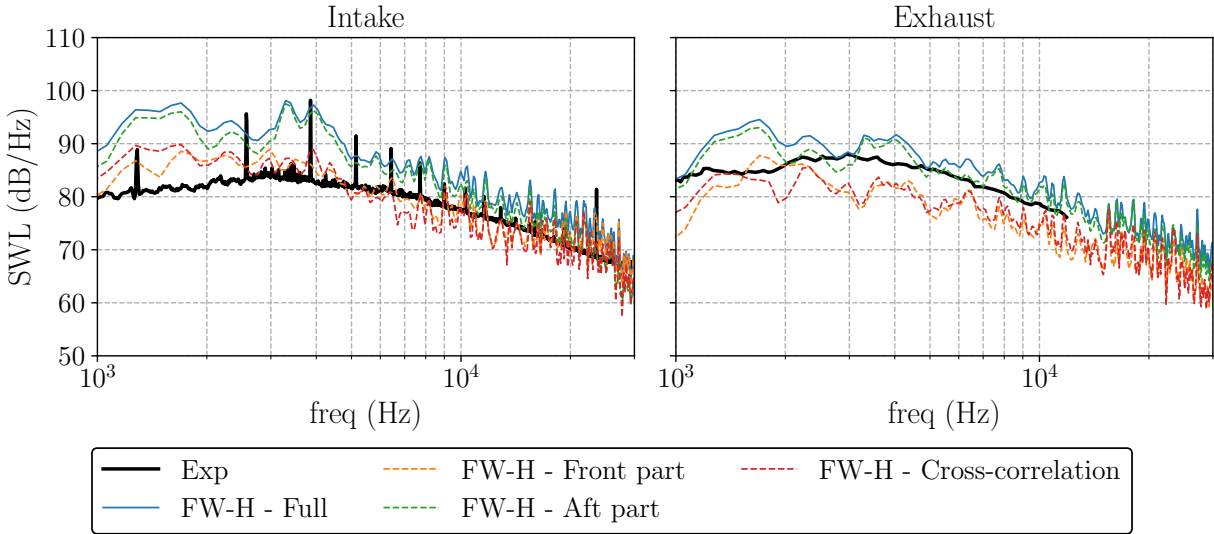


Figure 25 Upstream SWL (left) and Downstream SWL (right) spectra obtained from Ffowcs Williams and Hawkings analogy (10 windows).

indicate that the observed rear flow separation is less important in the experiment, and that it could be a consequence of a lack of mesh refinements on the vane surface. The cross-spectra also show that the upstream and aft part of the vane pressure fluctuations are correlated indicating a possible downstream shift of the RSI sources.

VIII. Conclusion

A comprehensive noise computation of the ACAT1 configuration at approach condition has been performed using a medium-sized mesh Large Eddy Simulation. The LES is in excellent agreement with the experimental performance parameters and with the hot-wire measurements, exhibiting small discrepancies within the experimental uncertainty for the latter. Significant disparities are however observed for the turbulence kinetic energy which seems to be overestimated by the simulation. Two hybrid noise computation methods have been used. The first is the LES-informed analytical model approach. The impact of the two available turbulent length scale estimates on the SWL has been studied, showing discrepancies at low frequencies that can be mainly attributed to the larger TLS estimate near the casing. This effect is however less important than for the corresponding RANS-informed study [9] because of the larger background TLS outside of the tip region, which seems to have counterbalanced it. Both Hanson's and Posson's models underestimate the noise levels on a large part of the studied frequency range. This underestimation may indicate the presence of additional noise sources in the experiment, which may not be negligible with respect to the RSI mechanism.

A higher order hybrid approach, coupling the LES with the Ffowcs-Williams and Hawkings analogy, has then been applied to assess the noise radiated by the stator row. A global overestimation of the radiated noise is observed, especially for the upstream prediction, which reveals discrepancies with the experiment that can reach 10 dB at low frequencies. The overestimation is mainly attributed to the fact that the FW-H analogy does not take into account the duct propagation effect. Moreover, it seems that the vane flow separation contributes more significantly than expected to the overall noise with respect to the RSI mechanism, which may indicate a need to refine the wall mesh in this zone to guarantee that it is well captured.

The under-prediction of the noise using LES-informed analytical models despite the over-predicted turbulence kinetic energy, in conjunction with an excessively overestimated noise using the FW-H analogy, which might be partly linked to an unexpected flow separation on the vane, support the hypothesis that a finer mesh is needed to draw reliable conclusions on the involved noise mechanisms. These observation also suggest that additional noise sources, such as the rotor leading edge flow detachment, may take part in the radiated noise in a significant way.

IX. Acknowledgments

The presented work was conducted in the frame of the project TurboNoiseBB, which has received funding from the European Union’s Horizon 2020 research and innovation program under grant agreement No. 690714.

This work was performed within the framework of the LABEX CeLyA (ANR-10-LABX- 0060) of Université de Lyon, within the program ‘Investissements d’Avenir’ (ANR-16- IDEX-0005) operated by the French National Research Agency (ANR).

The computational resources were provided by the GENCI network (CINES-OCCIGEN, project number A0062A06074) and by CERFACS.

The authors want to thank the members of the TurboNoiseBB consortium for providing experimental data and for fruitful discussions throughout the project.

The authors also want to thank Raphael Barrier (ONERA) for providing the rescaled OGV.

The authors are very grateful to Marlène Sanjosé (Université de Sherbrooke), for her precious advice about analytical models and for providing Université de Sherbrooke’s Ffowcs Williams and Hawkings’ analogy implementation. The numerous discussions on the subtleties of the FW-H analogy with Pavel Kholodov (Université de Sherbrooke) were also of great interest.

The authors want to thank Nicolas Odier and Maxime Fiore from CERFACS for their many advice on the meshing process and for the fruitful conversations on the use of AVBP and on the LES post-processing. The help from Florent Duchaine (CERFACS) for the application to obtain computational resources on GENCI’s cluster was also greatly appreciated.

Most of the LES post-processing was performed using Antares (release 1.13.0, <https://www.cerfacs.fr/antares>).

References

- [1] Moreau, S., “Turbomachinery noise predictions: present and future,” Vol. 1, No. 1, 2019, pp. 92–116.
- [2] Moreau, S., and Roger, M., “Advanced noise modeling for future propulsion systems,” *International Journal of Aeroacoustics*, Vol. 17, No. 6-8, 2018, pp. 576–599.
- [3] Peake, N., and Parry, A. B., “Modern challenges facing turbomachinery aeroacoustics,” *Annual Review of Fluid Mechanics*, Vol. 44, 2012, pp. 227–248.
- [4] Leonard, T., Sanjose, M., Moreau, S., and Duchaine, F., “Large Eddy Simulation of a scale-model turbofan for fan noise source diagnostic,” 2016, p. 3000.
- [5] Posson, H., Moreau, S., and Roger, M., “On the use of a uniformly valid analytical cascade response function for fan broadband noise predictions,” *Journal of sound and vibration*, Vol. 329, No. 18, 2010, pp. 3721–3743.
- [6] Masson, V., Posson, H., Sanjose, M., Léonard, T., Moreau, S., and Roger, M., “Fan-OGV interaction broadband noise prediction in a rigid annular duct with swirling and sheared mean flow,” *22nd AIAA/CEAS Aeroacoustics Conference*, 2016, p. 2944.
- [7] Ffowcs Williams, J. E., and Hawkings, D. L., “Sound generation by turbulence and surfaces in arbitrary motion,” *Philosophical Transactions of the Royal Society of London. Series A, Mathematical and Physical Sciences*, Vol. 264, No. 1151, 1969, pp. 321–342.
- [8] Goldstein, M. E., “Aeroacoustics,” *New York, McGraw-Hill International Book Co., 1976. 305 p.*, 1976.
- [9] Lewis, D., Moreau, S., and Jacob, M. C., “On the Use of RANS-informed Analytical Models to Perform Broadband Rotor-Stator Interaction Noise Predictions,” *25th AIAA/CEAS Aeroacoustics Conference*, 2019, p. 2667.
- [10] Meyer, R. K., Hakansson, S., Hage, W., and Enghardt, L., “Instantaneous flow field measurements in the interstage section between a fan and the outlet guiding vanes at different axial positions,” *13 th European Conference on Turbomachinery Fluid dynamics & Thermodynamics*, EUROPEAN TURBOMACHINERY SOCIETY, 2019.
- [11] Behn, M., and Tapken, U., “Investigation of Sound Generation and Transmission Effects Through the ACAT1 Fan Stage using Compressed Sensing-based Mode Analysis,” *25th AIAA/CEAS Aeroacoustics Conference*, 2019, p. 2502.
- [12] Tapken, U., Behn, M., Spitalny, M., and Pardowitz, B., “Radial mode breakdown of the ACAT1 fan broadband noise generation in the bypass duct using a sparse sensor array,” *25th AIAA/CEAS Aeroacoustics Conference*, 2019, p. 2525.

- [13] Brouwer, H., and Sijtsma, P., “Phased array beamforming to identify broadband noise sources in the interstage section of a turbofan engine,” *25th AIAA/CEAS Aeroacoustics Conference*, 2019, p. 2669.
- [14] Rai, M. M., and Madavan, N. K., “Multi-Airfoil Navier–Stokes Simulations of Turbine Rotor–Stator Interaction,” *Journal of Turbomachinery*, Vol. 112, No. 3, 1990, pp. 377–384.
- [15] Piomelli, U., “Large eddy simulations in 2030 and beyond,” *Philosophical Transactions of the Royal Society A: Mathematical, Physical and Engineering Sciences*, Vol. 372, No. 2022, 2014, p. 20130320.
- [16] Wagner, C., Hüttl, T., and Sagaut, P., “Large-eddy simulation for acoustics,” *Large-Eddy Simulation for Acoustics*, Vol. 9780521871, 2007, pp. 1–441. doi:10.1017/CBO9780511546143, URL <https://www.cambridge.org/core/product/identifier/9780511546143/type/book>.
- [17] Schönfeld, T., and Rudgyard, M., “Steady and unsteady flow simulations using the hybrid flow solver AVBP,” *AIAA journal*, Vol. 37, No. 11, 1999, pp. 1378–1385.
- [18] Lax, P. D., and Wendroff, B., “Difference schemes for hyperbolic equations with high order of accuracy,” *Communications on pure and applied mathematics*, Vol. 17, No. 3, 1964, pp. 381–398.
- [19] Nicoud, F., and Ducros, F., “Subgrid-scale stress modelling based on the square of the velocity gradient tensor,” *Flow, Turbulence and Combustion*, Vol. 62, No. 3, 1999, pp. 183–200.
- [20] Poinso, T. J., and Lele, S., “Boundary conditions for direct simulations of compressible viscous flows,” *Journal of computational physics*, Vol. 101, No. 1, 1992, pp. 104–129.
- [21] Odier, N., Sanjosé, M., Gicquel, L., Poinso, T., Moreau, S., and Duchaine, F., “A characteristic inlet boundary condition for compressible, turbulent, multispecies turbomachinery flows,” *Computers & Fluids*, Vol. 178, 2019, pp. 41–55.
- [22] Nicoud, E., Colin, O., Angelberger, C., Nicollet, F., and Krüger, C., “A no-slip implementation of a wall law boundary condition in a cell-vertex code for LES of internal aerodynamics on unstructured meshes,” *Conference LES4ICE, IFP Energies nouvelles, Rueil-Malmaison*, 2016.
- [23] Schmitt, P., POINSOT, T., Schuermans, B., and Geigle, K., “Large-eddy simulation and experimental study of heat transfer, nitric oxide emissions and combustion instability in a swirled turbulent high-pressure burner,” *Journal of Fluid Mechanics*, Vol. 570, 2007, pp. 17–46.
- [24] Wang, G., Moreau, S., Duchaine, F., De Laborderie, J., and Gicquel, L., “LES investigation of aerodynamics performance in an axial compressor stage,” *22nd Annual Conference of the CFD Society of Canada, Toronto, Canada, June*, 2014, pp. 1–4.
- [25] Wang, G., Moreau, S., Duchaine, F., Gourdain, N., and Gicquel, L., “Large Eddy Simulations of the MT1 high-pressure turbine using TurboAVBP,” *Proceeding of 21st Annual Conference of the CFD Society of Canada, Sherbrooke, Quebec, Canada*, 2013, pp. 70–106.
- [26] Kholodov, P., Pérez Arroyo, C., Sanjosé, M., and Moreau, S., “Fan Broadband Noise Computation at Transonic Regime,” *25th AIAA/CEAS Aeroacoustics Conference*, 2019, p. 2714.
- [27] Arroyo, C. P., Leonard, T., Sanjosé, M., Moreau, S., and Duchaine, F., “Large Eddy Simulation of a scale-model turbofan for fan noise source diagnostic,” *Journal of Sound and Vibration*, Vol. 445, 2019, pp. 64–76.
- [28] Odier, N., Duchaine, F., Gicquel, L., Staffelbach, G., Thacker, A., Rosa, N. G., Dufour, G., and Muller, J.-D., “Evaluation of Integral Turbulence Scale Through the Fan Stage of a Turbofan Using Hot Wire Anemometry and Large Eddy Simulation,” *ASME Turbo Expo 2018: Turbomachinery Technical Conference and Exposition*, American Society of Mechanical Engineers, 2018, pp. V02CT42A021–V02CT42A021.
- [29] Mockett, C., Knacke, T., and Thiele, F., “Detection of Initial Transient and Estimation of Statistical Error in Time-Resolved Turbulent Flow Data,” *8th International ERCOFTAC Symposium on Engineering Turbulence Modelling and Measurements*, , No. June, 2010.
- [30] Maunus, J., Grace, S., and Sondak, D., “Effect of CFD wake prediction in a hybrid simulation of fan broadband interaction noise,” *17th AIAA/CEAS Aeroacoustics Conference (32nd AIAA Aeroacoustics Conference)*, 2011, p. 2875.

- [31] Leonard, T., Sanjose, M., Moreau, S., and Duchaine, F., “Large Eddy Simulation of a scale-model turbofan for fan noise source diagnostic,” 2016, p. 3000.
- [32] Perot, F., Moreau, S., Kim, M.-S., Henner, M., and Neal, D., “Direct aeroacoustics predictions of a low speed axial fan,” *16th AIAA/CEAS aeroacoustics conference*, 2010, p. 3887.
- [33] François, B., Barrier, R., and Polacsek, C., “Zonal Detached Eddy Simulation of the Fan-OGV Stage of a Modern Turbofan Engine,” *ASME Turbo Expo 2020: Turbine Technical Conference and Exposition*, American Society of Mechanical Engineers Digital Collection, 2020.
- [34] Polacsek, C., Daroukh, M., François, B., and Barrier, R., “Turbofan Broadband Noise Predictions Based on a ZDES Calculation of a Fan-OGV Stage,” *9th Forum Acusticum*, 2020.
- [35] Pope, S. B., “Turbulent flows,” , 2001.
- [36] Jurdic, V., Joseph, P., and Antoni, J., “Investigation of rotor wake turbulence through cyclostationary spectral analysis,” *AIAA journal*, Vol. 47, No. 9, 2009, pp. 2022–2030.
- [37] Jaron, R., Moreau, A., and Guerin, S., “RANS-informed fan noise prediction: separation and extrapolation of rotor wake and potential field,” *20th AIAA/CEAS aeroacoustics conference*, 2014, p. 2946.
- [38] Hanson, D. B., “Theory for broadband noise of rotor and stator cascades with inhomogeneous inflow turbulence including effects of lean and sweep,” Tech. rep., 2001.
- [39] Posson, H., Roger, M., and Moreau, S., “On a uniformly valid analytical rectilinear cascade response function,” *Journal of Fluid Mechanics*, Vol. 663, 2010, pp. 22–52.
- [40] Posson, H., Moreau, S., and Roger, M., “Broadband noise prediction of fan outlet guide vane using a cascade response function,” *Journal of Sound and Vibration*, Vol. 330, No. 25, 2011, pp. 6153–6183.
- [41] Glegg, S. A., “The response of a swept blade row to a three-dimensional gust,” *Journal of sound and vibration*, Vol. 227, No. 1, 1999, pp. 29–64.
- [42] Kissner, C., Guérin, S., Seeler, P., Billson, M., Paruchuri, C., Carrasco Laraña, P., de Laborderie, H., François, B., Lefarth, K., Lewis, D., Montero Villar, G., and Nodé-Langlois, T., “ACAT1 Benchmark of RANS-informed Analytical Methods for Fan Broadband Noise Prediction: Part I - Influence of the RANS Simulation,” *Acoustics*, Multidisciplinary Digital Publishing Institute, 2020.
- [43] Fosso Pouangué, A., Sanjosé, M., Moreau, S., Daviller, G., and Deniau, H., “Subsonic jet noise simulations using both structured and unstructured grids,” *AIAA Journal*, Vol. 53, No. 1, 2015, pp. 55–69.
- [44] Casalino, D., “An advanced time approach for acoustic analogy predictions,” *Journal of Sound and Vibration*, Vol. 261, No. 4, 2003, pp. 583–612.
- [45] Najafi-Yazdi, A., Brès, G. A., and Mongeau, L., “An acoustic analogy formulation for moving sources in uniformly moving media,” *Proceedings of the Royal Society A: Mathematical, Physical and Engineering Sciences*, Vol. 467, No. 2125, 2011, pp. 144–165.
- [46] Ffowcs Williams, J. E., and Hawkins, D. L., “Sound generation by turbulence and surfaces in arbitrary motion,” *Philosophical Transactions of the Royal Society of London. Series A, Mathematical and Physical Sciences*, Vol. 264, No. 1151, 1969, pp. 321–342.